



## Modeling Continuum of Epithelial Mesenchymal Transition Plasticity

Journal:	<i>Integrative Biology</i>
Manuscript ID	IB-ART-09-2015-000219.R2
Article Type:	Paper
Date Submitted by the Author:	07-Dec-2015
Complete List of Authors:	Mandal, Mousumi; Indian Institute of Technology Kharagpur, School of Medical Science and Technology Ghosh, Biswajoy; Indian Institute of Technology Kharagpur, School of Medical Science and Technology Anura, Anji; Indian Institute of Technology Kharagpur, School of Medical Science and Technology Mitra, Pabitra; Indian Institute of Technology Kharagpur, Computer Science and Engineering Pathak, Tanmaya; Indian Institute of Technology Kharagpur, Department of Chemistry Chatterjee, Jyotirmoy; Indian Institute of Technology Kharagpur, School of Medical Science and Technology



Journal Name

ARTICLE TYPE

Cite this: DOI: 10.1039/xxxxxxxxxx

## Modeling continuum of epithelial mesenchymal transition plasticity<sup>†</sup>

Mousumi Mandal<sup>a</sup>, Biswajoy Ghosh<sup>\*,a</sup>, Anji Anura<sup>a</sup>, Pabitra Mitra<sup>b</sup>, Tanmaya Pathak<sup>c</sup>, and Jyotirmoy Chatterjee<sup>a</sup>

Received Date  
Accepted Date

DOI: 10.1039/xxxxxxxxxx

www.rsc.org/journalname

Living systems respond to ambient pathophysiological changes by altering their phenotype, a phenomenon called 'phenotypic plasticity'. This program contains information about adaptive biological dynamism. Epithelial-mesenchymal transition (EMT) is one such process found to be crucial in development, wound healing, and cancer wherein the epithelial cells with restricted migratory potential develop motile functions by acquiring mesenchymal characteristics. In the present study, phase contrast microscopic images of EMT induced HaCaT cells were acquired at 24 h intervals for 96 h. The expression study of relevant pivotal molecules viz. F-actin, vimentin, fibronectin and N-cadherin was carried out to confirm the EMT process. Cells were intuitively categorized into five distinct morphological phenotypes. A population of 500 cells for each temporal point was selected to quantify their frequency of occurrence. The plastic interplay of cell phenotypes from the observations was described as a Markovian process. A model was formulated empirically using simple linear algebra, to depict the possible mechanisms of cellular transformation among the five phenotypes. This work employed qualitative, semi-quantitative and quantitative tools towards illustration and establishment of the EMT continuum. Thus, it provides a newer perspective to understand the embedded plasticity across the EMT spectrum.

<sup>a</sup> School of Medical Science and Technology, Indian Institute of Technology Kharagpur, Kharagpur, India;

Tel: +91-3222-281225 ; E-mail: biswajoyghosh@smst.iitkgp.ernet.in

<sup>b</sup> Department of Computer Science and Engineering, Indian Institute of Technology Kharagpur, Kharagpur, India.

<sup>c</sup> Department of Chemistry, Indian Institute of Technology Kharagpur, Kharagpur, India.

<sup>†</sup> Electronic Supplementary Information (ESI) available. See DOI: 10.1039/b000000x/

**Insight, innovation, integration** Epithelial mesenchymal transition is a critical multi-step biological phenomenon, wherein the epithelial cells gradually develop motile characteristics in certain physiological and pathological conditions. Such an adaptive phenomenon has been proposed to progress through a continuum with epithelial-like and mesenchymal-like cells at two distinct ends and several intermediate phenotypic forms in between. In this study we have identified these intermediates from randomly selected representative populations in phase contrast images, estimated their conversion rates based on their frequency of occurrence and mathematically modeled their inter-conversion or in other words plasticity, along a temporal frame.

## 1 Introduction

Adaptation is a fundamental trait for any living organism. In order to fulfill this, both unicellular and multi-cellular species undergo morphological and physiological changes. The presence of several altered phenotypes coexisting in a population due to change in environmental conditions is called phenotypic plasticity<sup>1</sup>. The impact of such changes is reflected at the cellular and molecular levels of organization as well. Metazoan body organization comprises of epithelial and mesenchymal cells<sup>2</sup>. Epithelial Mesenchymal Transition (EMT) is a dynamic, cellular, multistep phenomenon where polarized, comparatively less migratory epithelial cells alter their morphology, intercellular connections, cytoskeletal organization, and gene expression to acquire mesenchymal phenotype with actively migratory and invasive behaviour<sup>3</sup>. E. D. Hay pioneered the study of EMT as a principal regulatory entity in embryogenesis<sup>4,5</sup>. Advancements in EMT research have demonstrated its role in wound healing<sup>6,7</sup>, fibrosis<sup>8–10</sup>, inflammation<sup>11</sup>, stemness<sup>12–15</sup>, and cancer metastasis<sup>16–18</sup>. Later on, the mirror phenomenon of mesenchymal epithelial transition (MET) was also reported<sup>19</sup>.

More recent developments in EMT research have indicated the existence of a fine interplay between the epithelial, mesenchymal and intermediate cells altering morphologically to adapt changes in microenvironment (like drug resistive response)<sup>20–22</sup>. Such an interdependent and partially complete phenomenon has been referred differently as epithelial mesenchymal plasticity (EMP)<sup>23</sup>, EMT-like phenomenon<sup>24,25</sup>, semi-mesenchymal phenotype<sup>22</sup>, hybrid phenotype<sup>21,26</sup>, intermediate phenotype<sup>27</sup>, and metastable stage<sup>28,29</sup>.

Limitations in clinico-pathological identification of EMT<sup>30–32</sup> has been attributed mainly to its extremely low cellular incidence and understanding of its heterogeneity<sup>20,33</sup>. Contemporary EMT developments have found highlights in *omics* research<sup>34–37</sup>, signaling pathway<sup>38,39</sup> and molecular marker studies<sup>40,41</sup>. Gene expression based kinetic models have been suggested to understand the switching among EMT phenotypes<sup>42–44</sup> and their stemness associations<sup>45</sup>.

In the present study (refer to ESI,† Fig. S1), cellular heterogeneity during EMT progression was documented from phase contrast images of *in vitro* EMT induced cells. The observations were supported by immunofluorescence (IF) labeling of filamentous actin (F-actin), vimentin, and fibronectin. Actin cytoskeletal protein regulates cell morphology and behavior which include shape, size, locomotion, and mechanotransduction<sup>46</sup>. It undergoes continuous remodelling during EMT<sup>47</sup>. Vimentin (also known as intermediate filament) is a cytoskeletal protein of mesenchymal cells regulating cellular shape, adhesion, migration and signaling<sup>48,49</sup>. Fibronectin, on the other hand, is an extra cellular matrix (ECM) protein that plays a major role in cell adhesion, migration, and differentiation<sup>50</sup>. This dual-level finding of

EMT manifestation was further validated by expression study of N-cadherin in addition to vimentin and fibronectin. N-cadherin is a cell junctional protein expressed in mesenchymal cells<sup>51</sup>.

Thus a critical modeling of cellular plasticity within the intermediate stages of EMT axis was attempted using simple linear algebra based discrete Markov model. Markovian models range from simple Markov chains to discrete, hidden or random field models<sup>52</sup>. The fundamental theory behind any Markovian process is the satisfaction of what is called the "Markov property" which states that the conditional prediction for the occurrence of a future event depends entirely on the present state and not the series of preceding states. Being a probabilistic model, it enjoys a range of applications in real world problems including weather forecast, signal processing, artificial intelligence, finance, computational research to name a few. In this paper we exploit discrete Markov tools to identify the dynamism displayed by the cells while undergoing EMT. This may have important implications in aiding histopathologists to appreciate EMT in their routine practices.

## 2 Methods

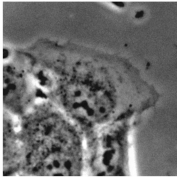

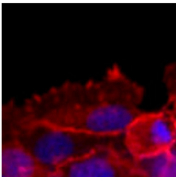
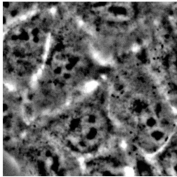

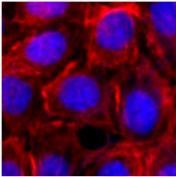
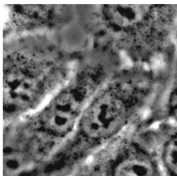

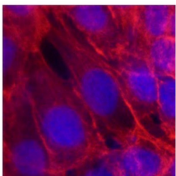
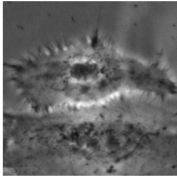

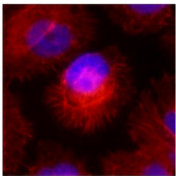
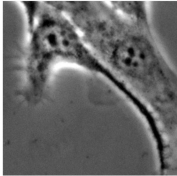

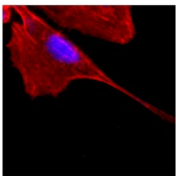
A flow diagram briefing the experimental steps for the work has been elaborated (refer to ESI,† Fig. S2).

### 2.1 HaCaT culture and EMT induction

HaCaT cells (Human keratinocyte cell line procured from National Centre for Cell Science, Pune, India) were cultured in Dulbecco's modified Eagle's medium (DMEM) (HiMedia, India) with 10% fetal bovine serum (FBS) and 1% antibiotic solution (HiMedia), maintained at 5% CO<sub>2</sub> and 37°C. About  $1.0 \times 10^4$  per cm<sup>2</sup> cells were seeded on cell culture plates. 50% confluent cells were serum starved and treated with 2 ng/ml of transforming growth factor - beta 1 (TGF -  $\beta$ 1) (HiMedia) and 10 ng/ml of epidermal growth factor (EGF) (Sigma, USA) in serum free DMEM for EMT induction. The EMT changes were monitored for 96 h after growth factor treatment. HaCaT cells without treatment were taken as '0' h study group. This group has been considered as the control throughout. For the purpose of experimental validation, a second cell line (AW13516- human tongue squamous cell carcinoma, provided by Dr. Milind Vaidya, ACTREC, Mumbai, India) was tested using the protocol.

### 2.2 Phase contrast imaging

The morphological changes of EMT in HaCaT cells were monitored at 24 h intervals for 96 h by acquiring microphotographs under an inverted phase contrast microscope (Zeiss Observer Z1, Carl Zeiss, Germany) with 10 $\times$  objective (NA 0.25) and a CCD camera (Model: AxioCam MRm) with final magnification 100 $\times$ . Phase contrast microscope images were grabbed from a random region of interest consisting of evenly distributed cells through-

Phase Contrast Image	Target Cell Schematic (Not to Scale)	F- Actin Expression	Observed Cell Attributes	Phenotype-based Nomenclature
			<ul style="list-style-type: none"><li>• Polygonal cells.</li><li>• Marginally located in cell cluster.</li><li>• Partial perimetric interface with neighbouring cells.</li><li>• Presence of a free undulated margin with lamelliopodia.</li><li>• Limited Inter-cellular Space (ICS)</li><li>• Actin filaments arranged beneath the plasma membrane: branched near lamelliopodia and belt like along neighbouring interfaces.</li></ul>	$\alpha$
			<ul style="list-style-type: none"><li>• Polygonal cells with smooth margin.</li><li>• Complete perimetric interface with neighbouring cells.</li><li>• Limited ICS.</li><li>• Actin filaments localized as cortical actin belts.</li></ul>	$\beta$
			<ul style="list-style-type: none"><li>• Spindle or dumbbell shaped cells with smooth margin.</li><li>• Perimetric interface with the neighbouring cells more than alpha but lesser than beta.</li><li>• Less ICS.</li><li>• Actin filaments are present near the plasma membrane.</li></ul>	$\gamma$
			<ul style="list-style-type: none"><li>• Stellate cells with radiating margin due to formation of multiple filopodias.</li><li>• Perimetric interface with neighbour is lesser than alpha, beta, and gamma.</li><li>• High ICS.</li><li>• Actin filaments bundled to support filopodias.</li></ul>	$\delta$
			<ul style="list-style-type: none"><li>• Fusiform cells with a characteristic tail and lamelliopodia in opposite sides (resembling front-rear polarity).</li><li>• Limited perimetric interface with neighbour cells.</li><li>• Highest ICS.</li><li>• Polymerized actin filaments forming parallelly-aligned fibres in cytoplasm, oriented along the cell major axis.</li></ul>	$\epsilon$

**Fig. 1** Visual classification and nomenclature of HaCaT cells undergoing EMT on the basis of observed morphological and F-actin expression features from representative cell population.

out.

### 2.3 Immunofluorescence (IF) labelling

Cells were fixed in 4% paraformaldehyde for 15 minutes and permeabilized with 0.25% Triton X-100 in PBS for 5 minutes. Rhodamine-phalloidin (Cat. No. R415, Molecular Probe, USA) was used to visualize Actin filaments. Cells were blocked with 10% goat serum in 1% bovine serum albumin in PBST and immunostained with mouse anti-human vimentin monoclonal antibody (Cat. No. [RV202] (ab8978), Abcam, UK) and rabbit anti-human fibronectin polyclonal antibody (Cat. No. (H-300): sc-9068, Santa Cruz Biotechnology, USA). After a series of PBS wash, cells were incubated with Alexa Fluor®594 conjugated goat anti-mouse secondary antibody (Cat. No. A-11005, Molecular Probe) and Alexa Fluor® 488 conjugated goat anti-rabbit secondary antibodies (Cat. No. A-11008, Molecular Probe) for 1 h. Cells were counterstained with DAPI (4', 6-diamidino-2-phenylindole) (Sigma-Aldrich, USA). Microphotographs were taken under Zeiss Microscope (Zeiss Observer Z1, Carl Zeiss, Germany) in fluorescence mode with 20× objective (NA 0.40), CCD camera (Model: AxioCam MRm) with the total magnification of 200×.

### 2.4 Quantitative Real Time Polymerase Chain Reaction (qRT-PCR) for gene expressions

Total RNA of untreated and treated cells at different temporal points (0, 24, 48, 72, and 96 h) were extracted by Trizol reagent (Life Technologies, USA) by following manufacturer's instructions. Complementary DNA (cDNA) was synthesized by reverse transcription of mRNA using cDNA synthesis kit (Promega, USA) in Arktik Thermal Cycler (Thermo Fisher Scientific, USA). qRT-PCR was performed for the quantification of genes —vimentin, fibronectin, and N-cadherin in the LightCycler LC480 (Roche Diagnostics, Germany) using Light Cycler Fast Start DNA Mastermix - iQTM SYBR Green Supermix (BIO-RAD, California, USA). 18S rRNA gene was taken as an endogenous control. Each sample was taken in triplicate reactions. Primer sequences, annealing temperature and their cycling conditions are mentioned in ESI,† Table S1. The expression analysis study was based upon the relative-quantification method<sup>53</sup>.

### 2.5 Cell population analysis

Bias minimization in this study of phenotypic state changes among the selected representative cell population was achieved by random sampling. A group of 100 cells was selected (phase contrast images) from each of the five microscopic field of view (1040 x 1388 pixels, 10× objective). Thus, from each time point, 500 cells were used in this study. This kind of sampling was repeated at different temporal points of 24 h interval for a period of 96 h (i.e. images were acquired at 0, 24, 48, 72, and

96 h). Thus, a total of 2,500 randomly selected cells were studied to understand and model the phenotypic plasticity of cells. Based on cell size, cell shape, membrane roughness (podia structures), and intercellular interactions, all the cells marked (refer to ESI,† Fig. S3) at specified time points were visually classified into five phenotypic groups (viz.  $\alpha$ ,  $\beta$ ,  $\gamma$ ,  $\delta$ , and  $\epsilon$ ) (Fig. 1). However, in our experiment, 2-4 among 100 cells (as our region of interest) were found to exhibit ambiguous morphology i.e. a phenotype showing mixed characteristics. To address this, we have considered two features in the order of importance - shape and peripheral podia structure. This was done since change in shape symmetry and development of migratory structures (podia) are strongly indicative of EMT. The morphological attributes of the cell phenotypes- area, perimeter, major to minor-axis ratio, and eccentricity were quantified and statistically validated to differ visibly among the cell categories in Matlab®R2014b platform (image processing, statistics and machine learning toolbox) (refer to ESI,† Fig. S4). The population was analyzed using cell frequency plot and a probabilistic model was created to describe the EMT plasticity.

## 3 Results and Discussions

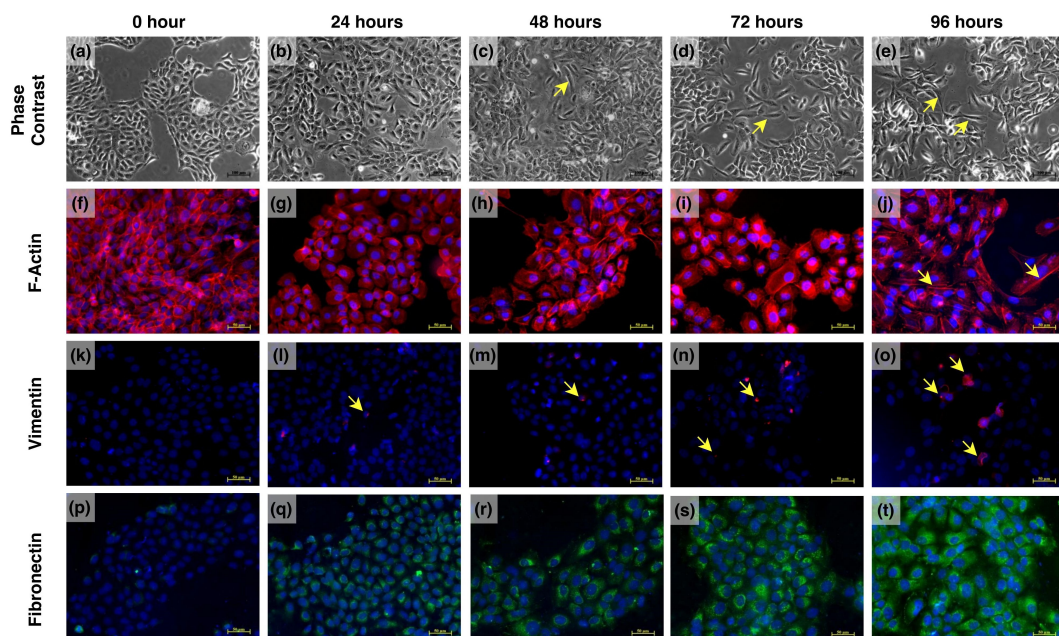
### 3.1 EMT and its plasticity

#### 3.1.1 Morphological plasticity

The morphological changes in EMT-induced HaCaT cell population was assessed from phase contrast images. It revealed changes in cellular shape, size, and connectivity (Fig. 2 a - e). In the untreated condition (Fig. 2 a) almost all the cells appeared polygonal and cobblestone in shape. They were closely connected to each other displaying colonial patterns (epithelial sheet-like monolayer arrangement). However, post treatment, a subset (subset gradually expanding with time) of the population acquired elongated shape (marked by arrows in Fig. 2 c, d, e), loosely attached to neighbouring cells and were dispersed throughout the microscopic field of view. Such an event was indicative of mesenchymal morphology. These observations were found to be corroborative with previous in vitro studies<sup>54-56</sup>. Although subtle changes were noticeable from 24 h (Fig. 2 b) of intervention itself, marked phenotypic changes were observed 48 h onwards (Fig. 2 d, e) post EMT induction.

#### 3.1.2 Behavioral plasticity

Morphological and migratory structure alterations were evaluated with IF labelling of F-actin. Immunofluorescence micrographs (Fig. 2 a-e) exhibited changes in localization, orientation, and organization of F-actin in EMT induced HaCaT population. F-actin molecules in the untreated condition were found to be localized in close proximity to the cell membrane (Fig. 2 f), also referred to as cortical actins<sup>46,56</sup>. The actin filaments forms stress fibres during EMT induced by TGF- $\beta$ 1<sup>56,57</sup>. In the present



**Fig. 2** Figure illustrating morphological changes, population heterogeneity, and relevant molecular expression during EMT (EMT was induced in HaCaT population by TGF- $\beta$ 1 and EGF) at different time points. (a-e) Phase Contrast micrographs (Objective 10  $\times$ ). The arrows indicate occurrence of elongated mesenchymal-like cells (c-e). (f-t) Immunofluorescence micrographs\* showing progressive molecular expression of (f-j) F- Actin (red), (k-o) Vimentin (red), (p-t) Fibronectin (green) at 20  $\times$  objective magnification. The arrows indicate the development of stress fibers (j) and vimentin expression (l-o). (\*DAPI was used for nuclear staining (blue))

study, F-actin gradually formed thick bundles, parallelly aligned throughout the cytoplasm with treatment of TGF- $\beta$ 1 and EGF in progressing time intervals (Fig. 2 g, h, i, j). Actin forms the backbone to lamelliopodia and filopodia<sup>58</sup>. At 48 h (Fig. 2 h) and 72 h (Fig. 2 i), bundled actin were observed to strengthen the newly formed filopodias. Stress fibres were clearly observed at 96 h image frame (indicating arrows Fig. 2 j). These fibres were found to connect the focal adhesion points of cell membrane, oriented parallel to the longitudinal axis of cells (Fig. 2 j). This observation is well backed by the fact that stress fibres are responsible for maturation of focal adhesions<sup>59</sup>. Hence, morphological and behavioural modifications were found in the HaCaT cells during the in vitro EMT experiment.

3.1.3 Molecular plasticity

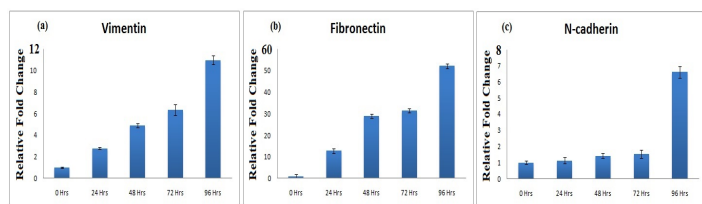
The incidence of EMT in the cells was validated by molecular expressions of vimentin and fibronectin through IF labelling. Additionally, qRT-PCR was performed with N-cadherin in addition to vimentin and fibronectin. In vitro and in vivo studies have reported that vimentin is expressed during EMT and possess strong correlation with mesenchymal morphology during tumor progression<sup>60–63</sup> and migratory behavior of cells in wound and cancer<sup>48,64,65</sup>. In our experiment, IF labelling of vimentin demonstrated a progressive up-regulation in vimentin expression (Fig. 2 k-o), corroborative with the fold changes as seen in qRT-PCR

(Fig. 3 a). The untreated cells showed almost no sign of vimentin expression. The 24 –72 h temporal window witnessed vimentin expression limited to the perinuclear region. However, at 96 h, it was observed to be distributed throughout the cell, possibly to reinforce cytoskeletal networks as reported by Tirino *et al.*,2013<sup>66</sup>.

The expression of fibronectin during EMT in the HaCaT population illustrates a step-wise but rapid increment (Fig. 2 p-t and 3 b). Though fibronectin is principally secreted by fibroblast into ECM, it is also synthesized in keratinocytes after stimulation by TGF- $\beta$ <sup>67</sup>. Recent study on breast epithelial cell line (MCF-10A) illustrated the time dependent increase of fibronectin expression during EMT induction, also responsible for cell migration<sup>68</sup>. Fibronectin, being an ECM protein, ensures the preference of cell-ECM interaction over cell-cell interaction with its elevated expression. More ECM-cell interaction is indispensable for cellular migration of  $\delta$  and  $\epsilon$  cells.

Furthermore, qRT-PCR results displayed a sudden up-regulation of N-cadherin. Cadherin switching from E-cadherin to N-cadherin is a common phenomena in carcinoma as well as EMT<sup>69,70</sup>. N-cadherin has been considered to form dynamic cellular associations which execute both attachment and detachment during migration<sup>71</sup>. On the other hand, N-cadherin —F-actin dynamism was reported to be essential during collective migration<sup>72</sup> and regulated by Rho GTPase<sup>73</sup>. It was found that N-





**Fig. 3** Gene expression profile of vimentin, fibronectin, N-cadherin at 0, 24, 48, 72, 96 h of EMT progression in HaCaT population.

cadherin expression was consistently low up to 72 h (Fig. 3 c). However, a substantial but sudden rise was observed at the 96 h time frame. Sudden increase in N-cadherin expression might be indicative of collective migration executed by  $\alpha$  and  $\delta$  cells beside individual migration by the  $\epsilon$  cells.

There is a trend of gradual change in molecular expression of EMT marker genes in a population. But the degree of how gradual it is, subjectively varies. The expression of fibronectin was found to be fast with a substantially high magnitude. On the other hand vimentin and N-cadherin expressions were moderate to slow as is depicted in IF and qRT-PCR results. The vimentin expression was not as prominent as fibronectin which concurs to previous in vitro studies<sup>74</sup>. Thus, this study correlates three EMT-associated cardinal gene expressions, with the changed cellular phenotype and migratory potential of the cells. The molecular expression of vimentin was performed in AW13516 (refer to ESI,† Fig. S5d-f) to confirm EMT progression. In this carcinoma cell, perinuclear vimentin expression was found in control (0 h), gradually acquiring a partial spread-out appearance by 48 h of intervention.

Phase contrast micrographs of AW13516 (refer to ESI,† Fig. S5a-c) indicated prominent changes from 24 h. Most cells at 48 h were detached from substratum for acquiring a migratory phenotype. Being a cancer cell line, the changes observed were found to be more rapid compared to a normal cell line.

## 3.2 The continuum of EMT

### 3.2.1 Phenotypic continuum

All the cells were classified on the basis of their shape, intercellular space (ICS), migratory structures and F-actin configuration (Fig. 1). The cells showing highest resemblance to epithelial properties were designated as 'epithelial' phenotype or  $\beta$ . These cells were polygonal shaped; with least ICS i.e. closely packed neighboring cells. Additionally, the F-actin IF micrographs revealed its cortical distribution. The next category of cells demonstrated mostly epithelial-like properties infused with some mesenchymal traits. These were named as 'epithelial-like' phenotypes or  $\alpha$ . The  $\alpha$  types were polygonal shaped that were marginally located and expressed partial migratory structures (lamelliopodia-like) on the free surface. The actin filaments near the free surface

were branched, but were otherwise cortically distributed. 'Progressive mesenchymal' phenotypes or  $\gamma$  were the cells with comparable levels of epithelial and mesenchymal traits with slightly higher epitheliality. The cells bore non-epithelial characters like elongated dumbbell/spindle shape. Conversely, they exhibited smooth surface devoid of noticeable migratory structure, low ICS, and presence of cortical F-actin as non-mesenchymal features. The phenotypes that resembled relatively higher mesenchymal traits were referred to as 'mesenchymal-like' or  $\delta$  cells. These cells were stellate shaped with distinct migratory structures all around (filopodia), sparsely distributed in the microscopic field of view. The actin bundles fortified the filopodia, as observed in the IF. Lastly, the category of cells with the most mesenchymal features was the 'mesenchymal' phenotype or  $\epsilon$ . Apart from its fusiform shape (distinctly tailed) and high ICS, prominent migratory structures (lamelliopodia and filopodia) were observed. IF of vimentin and fibronectin supports the evidence of cells acquiring mesenchymal phenotype towards the advanced temporal points (Fig. 2 k-t).

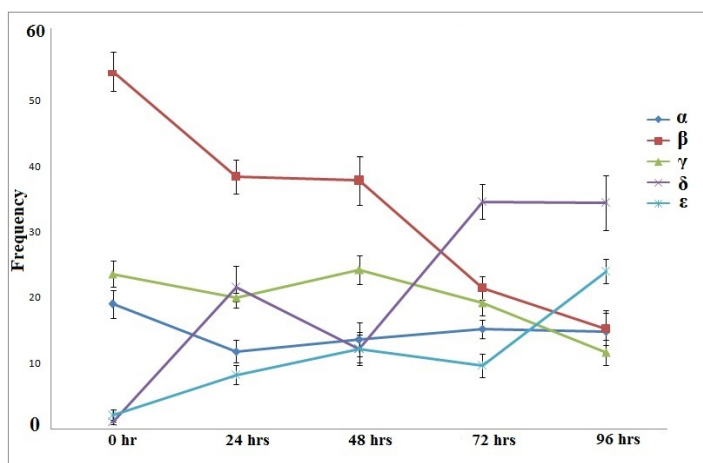
### 3.2.2 Morphometric continuum

The morphological attributes of the cell phenotypes- area, perimeter, major-minor axis ratio, and eccentricity were quantified and statistically validated to differ visibly among the cell categories (refer to ESI,† Fig. S4). It was found that the features that showed good demarcation among phenotypes were major to minor axis ratio and the eccentricity. Since both the features are representative of how elongated the cells are, it can be inferred that the phenotypes gradually acquire an elongated morphology as they further progress along the EMT timeline. It is to be noted that based on quantified cell morphometric variations across phenotypes along with their visual features and migratory behavior, the transition may be broadly stated as a lineage in the order  $\beta \rightarrow \alpha \rightarrow \gamma \rightarrow \delta \rightarrow \epsilon$ .

## 3.3 EMT heterogeneity and dynamism

### 3.3.1 Dynamism in cell population

The salient observations of the population plot (Fig. 4) unveiled some notable findings (Table 1): (i) prominence in the number of  $\beta$  cells at initial stages and a step-wise decrease in its frequency with advancement of time, (ii) maintenance of average cell number among the  $\alpha$  and the  $\gamma$  subset, (iii) a mirror-like symmetrical relation observed between the  $\beta$  and the  $\delta$  phenotypes, (iv) the prevalence of the  $\delta$  and the  $\epsilon$  cells towards the terminal phase of the experiment. The slopes of curves during each interval were used as a measure to empirically estimate the probable tendencies of phenotypic plasticity across the whole range of 96 h.



**Fig. 4** Frequency of cell phenotype ( $\alpha, \beta, \gamma, \delta, \epsilon$ ) at different temporal points (24 h interval) during EMT. The high prevalence of the  $\beta$  cells and its gradual decrease was suggestive of its 'epitheliality'. Conversely, the extremely low number of the  $\delta$  and the  $\epsilon$  at the beginning and high occurrence towards the end marks their 'mesenchymality'. The  $\alpha$  and the  $\gamma$  subtypes maintained a low rate of change in frequency with time throughout the entire timeline.

### 3.4 Mathematical model

To understand the plasticity continuum during EMT and the temporal interplay of intermediate phenotypes, we modeled the cellular transitions. The hypothesis of the model follows Markovian process in which the distinct number of states undergoes change at equal intervals of time. Such changes occur from one state to other (here a state resembles a cell phenotype) with the origin state being epithelial cells. Each transition is denoted with its respective state transition probability that predicts the probable tendency of each phenotype (state) to the next eventually leading to the formation of the goal state (mesenchymal cells). It is to be noted that in biological systems during EMT, cell cycle arrest occurs, our experimental protocol has taken this under consideration. In our *in vitro* experiment, serum starvation and application of TGF- $\beta$ 1 were responsible for arresting the cell cycle and progressively inducing mesenchymality. In normal epithelial tissues and initial stages of cancer it has been found that TGF- $\beta$  is a tumor suppressor (arresting cell cycle)<sup>75</sup>. Furthermore, it also acts as pro-metastatic factor (promoting EMT)<sup>76–78</sup>. At this stage TGF- $\beta$  has been studied to show anti-apoptotic role by increased expression of anti-apoptotic factor DEC1<sup>79</sup>. Hence, with our experimental framework we have minimised the incidence of cell proliferation and apoptosis. Thus while modeling, it was assumed that the state transitions among phenotypes as the predominant players in population plasticity. In order to simplify computation and provide an overall picture we used linear matrix algebra to estimate the state transition weights.

To describe EMT and the changes occurring in their population temporally, Markovian process was deployed. Similar to the discrete Markov process, this study of EMT, consists of five ( $N = 5$ ) observable states ( $S = \alpha, \beta, \gamma, \delta, \epsilon$ ) at the five equally spaced time points ( $t = 0, 24, 48, 72, 96$ ). At a fixed time the overall representation of the states may be denoted as  $X_t$ . The system undergoes a change in phenotype according to a set of probabilities associated with the state. Additionally, the population specifications of each phenotype at the current and all the preceding time frames can provide a full probabilistic description of the current states<sup>52</sup>. Thus, the probability description can be given as:

$$P[X_t = S_n | X_{(t-1)} = S_{(n-1)}, X_{(t-2)} = S_{(n-2)} \cdots, X_0 = S_0] \quad (1)$$

Additionally, following from Eq. (1) each state change in a given interval is denoted with a state transition probability  $a_{(n1,n2)}$  of the form

$$a_{(n1,n2)} = P[X_t = S_n | X_{(t-1)} = S_{(n-1)}] \quad (2)$$

where  $n1, n2$  are the phenotypic states that may or may not have changed in a single time interval.

Here, in this work, we have used state transition weights ( $w_{(n1,n2)}$ ) as a representative of state transition probability ( $a_{(n1,n2)}$ ) after observing the phenotypic modifications during EMT for a total of 2500 cells. The task of obtaining the values of ( $w_{(n1,n2)}$ ) for a phenotype change (due to switching and phenotypic plasticity) was performed in several steps of evaluation. Cell number ( $F$ ) vs. time ( $t$ ) was plotted for all the cells to estimate the number of cells of a phenotype at a given time in the population. The slope (or the rate constant ( $k$ ) for first order) of the curve of increasing/decreasing number for a given phenotype (Table 1) was determined at every interval.

$$\frac{dF_{(n1,n2)}}{dt} = k_{(n1,n2)} \quad (3)$$

Since the system was completely conserved (i.e. each time point has a fixed number of 500 cells), an increased frequency of a phenotype will correspond to the decreased frequency of another, i.e. the sum of all the rate constants will be zero.

$$\sum_{i=1}^5 k_i = 0 \quad (4)$$

where,  $i$  is the number of phenotype changes within an interval.

On evaluation of the specific rate constants, all the phenotypes with a positive slope were designated as 'forming cells'. Alternatively, the negatively sloped phenotypes were the 'contributory cells'. In other words the assumption that the contributory cells ( $c$ ) underwent plasticity by phenotypic switching to give rise to the newly forming cells ( $f$ ) was the basis of our hypothesis to



**Table 1** Rate of change of the five cellular phenotypes elucidating their interplay during EMT for a period of 96 h for 500 cells (100 cells each randomly collected from five phase contrast images in three experimental trials). The table demonstrates the rate of formation or decline of cell phenotypes as observed in the four studied intervals in a fully conserved system i.e.  $\frac{dF_{(n1,n2)}}{dt} = k_{(n1,n2)}$  is always equal to zero. ( $F$ : cell number,  $i$ : time interval in hours,  $t$ : time and  $k$ : cell growth/decline rate constant.)

Phenotypes	$\Sigma(k_i * 24)$			
	i=0-24	i=24-48	i=48-72	i=72-96
alpha	-36	9	7	-1
beta	-80	-3	-81	-32
gamma	-18	21	-25	-38
delta	103	-47	112	-1
epsilon	20	20	-13	72

map the dynamism of this phenomenon.

$$[f_i] = \begin{bmatrix} k_{1i} & k_{2i} & k_{3i} \end{bmatrix} \begin{bmatrix} c_1 \\ c_2 \\ c_3 \end{bmatrix}$$

where,  $1 \leq i \leq 5$  and  $k_{1i}, k_{2i}, k_{3i}$  are the estimated state transition weights  $w_{(n1,n2)}$  in which the contributory phenotypes  $c_1, c_2, c_3$  (in this case) produced the  $i$ th forming phenotype respectively. It is to be noted that the contributory and forming cells were allocated purely on the basis of time rate of change among the phenotypes. The observed transitions with assigned weights were estimated (Table 1). Furthermore, transitions were categorized as strong, moderate, and weak based on the assigned values (observed as solid, thick dotted and dotted line respectively in Fig. 5). A 3-fold cross validation was performed on a disjoint set of cells collected by the same sampling method with 200 cells in each fold (refer to ESI,† Fig. S6) to test the model coefficients for each of the four time intervals. The sampling method helped minimizing the bias to reduce error. At the same time, the relatively high sample size to feature dimensionality ratio was instrumental to counter overfitting of the model. Prediction of the model was estimated on the mean population and the error values were calculated (Table 2). Furthermore the model can provide us with probabilities of a future state conditionally based on the preceding observation given as:

$$P[O|Model] = P[s_1, s_2, s_3, \dots, s_n | Model] \quad (5)$$

where,  $O$  is the observation and  $s_n$  is the state of the phenotype in the  $n$ th observation.

Although EMT broadly occurs via a progressive directionality as pointed out in previous sections, an interesting interplay is observed between the phenotypes endorsing the dynamism of

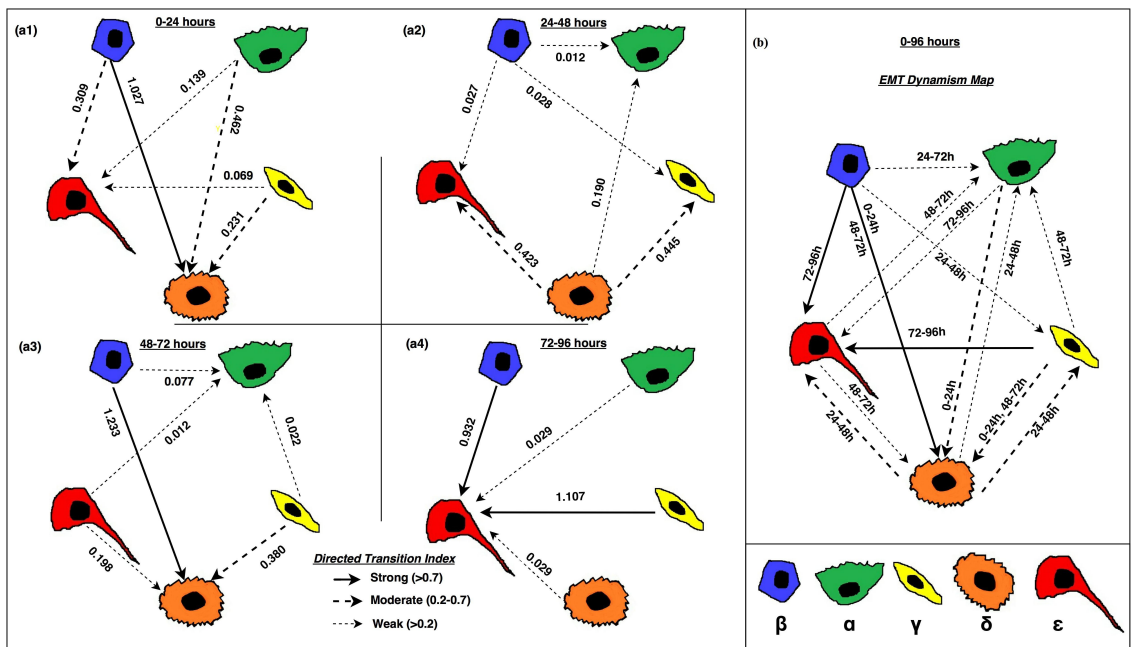
**Table 2** Error estimation during four intervals to evaluate/predict forming-cell frequencies using state transition weights (established from model) on the central tendency (mean) of five experiments each containing 100 cells. (Dependent variable range = 0-100).

Interval (hours)	MSE	RMSE
0-24	0.076	0.276
24-48	0.033	0.182
48-72	0.078	0.279
72-96	0.202	0.450

the cell plasticity. The step-like changes in the  $\beta$  phenotype is one of such observations. This may be suggestive of marked alternating ‘active-passive-active’ trends in them. During the occasion of passiveness among  $\beta$  states, a marked increase in the other transient states may be indicative of compartmentalization of role for each phenotype. This kind of distributed delegation of load reduces the continuous pressure on the epithelial phenotype ( $\beta$ ) and ensures an order in the entire transition, visually analogous to looping-earthworm movement. The state transition diagram shows that the  $\beta$  cells never belong to the ‘forming’ subset of cells and has strong contributory role in the intermediate mesenchymal-like ( $\delta$ ) and terminal mesenchymal ( $\epsilon$ ) phenotypes. However, even though weak, it has contributory effect towards formation of the epithelial-like ( $\alpha$ ) and progressive mesenchymal ( $\gamma$ ) as well. These demonstrate stemness among the  $\beta$  cells in terms of being a source to all other sub-population but formed by none. While major incidences of cancer stem cell (CSC) have been reported to be mesenchymal in nature, one of its many reasons is attributed to the EMT process itself contributing to the generation of CSC<sup>13,80</sup>. However, notionally, CSC has multiple origins<sup>81</sup>. Normal stem cells have also been seen to be one of the sources of CSC. But the relation is not one to one. Normal stem cells, after several steps of differentiation form CSC<sup>82</sup>. In our in vitro experiment,  $\beta$  cells in initial population bear a certain degree of “stemness” as exhibited by the tissue resident stem cells.  $\beta$  cells demonstrating the property of stemness has thus been derived from the perspective of normal epithelial stem cell as it gives rise to other cell phenotypes ( $\alpha, \gamma, \delta, \epsilon$ ) without any evidence of it being formed by the other phenotypes.

A typical mirror-like symmetry observed between the  $\beta$  and the  $\delta$  phenotypes, intersecting at around (60 h), suggested a highly coordinated and complementary switching between the two. Furthermore, the terminal mesenchymals ( $\epsilon$ ) that was lying dormant all this time started to show increment after 72 h (right after the establishment of predominance in  $\delta$  cells over the other near-epithelial phenotypes i.e.  $\beta, \alpha, \gamma$ ). The  $\alpha$  and the  $\gamma$  sub-population maintained a nearly similar but low-levels of frequency, like a cell-bridging buffer.

The hypothesis that EMT is a multistep dynamic process, ob-

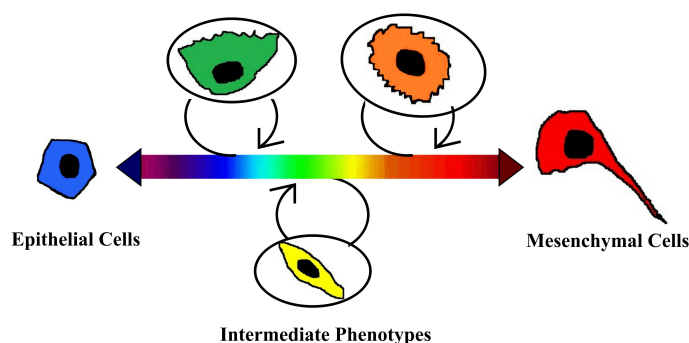


**Fig. 5** Modeling of phenotypes along with the state transition weights to denote the strength of plasticity.

servable at the cellular dimension was proved with a multitude of approaches. The a priori knowledge of the phenomenon lead us to assume that the progression of EMT will reveal certain degrees of diversity among the transforming cells as each of them will be responding differently to the induction depending on their microenvironment and adaptive needs<sup>22,27,83</sup>. According to the theory of phenotypic plasticity in biology, an altered ambience impacts the living entities to change differently<sup>1</sup>. In times of strong phenotype to environment stimuli a highly variable response is observed among the phenotypic entities<sup>84</sup>. In many cases switching between phenotypes has also been reported at the gene level<sup>42</sup>, implying the interdependence of phenotypes in an enclosed population during the transition from one equilibrium (stable) state to the other. In this case the epithelial and mesenchymal states were the stable states for the cells. Post induction, the cells exhibiting differential phenotypic properties were sampled at selected time points to observe their individual as well as relative changes. We broadly classified the phenotypes in five morphological categories and critically observed their relative changes in frequency. The actual process of EMT was confirmed using immunofluorescence of F-actin, vimentin, and fibronectin and marker gene expression analysis. Using semi-quantitative tools we estimated the morphological parameters of our five study components and based on their structural closeness in terms of surface smoothness, neighborhood interaction and elongation we primarily concluded a possible lineage of cell development from epithelial to mesenchymal type i.e.  $\beta \rightarrow \alpha \rightarrow \gamma \rightarrow \delta \rightarrow \epsilon$ . On

further evaluation of the outcome of phenotypic frequency at progressive temporal locations, we obtained subtle to strong evidences to infer interplay of phenotypic plasticity including switching between them and moving to and fro along the EMT axis (not just a linear chain of transitions) (Fig. 6). The linear transition sequence is a representation strictly based on progressive alterations in morphological properties of phenotypes. This is done to demonstrate how based on the increasing value of mesenchymal cell features like major-minor axis ratio and eccentricity, how the transition from an epithelial to mesenchymal is expected to progresses. However, the Markovian model demonstrates a more holistic way to illustrate how the transition actually may occur among the phenotypes, as a population (i.e. through a dynamic continuum) (Fig 5) and not as a single set of same phenotype cells.

The study of cell populations indicated a dynamic interplay of phenotypes. This led to the idea of modeling the temporal changes and their interdependence. As the state transitions among the phenotypes with time was the primary basis of our model, we chose Markovian laws to explain the phenomenon. The Markovian process is a simple probabilistic modeling that predicts the future outcome of a given state based on the prior likelihoods (state transition coefficients) of a state to occur (new phenotype) given that it was previously in another state (preceding phenotype). The weights provided a distinguishing insight into the phenotype switches and their interdependent temporal behavior.



**Fig. 6** Simplified schematic representing interplay of different phenotypic forms along the EMT spectra. An analogy has been drawn between EMT continuum and the electromagnetic spectrum of visible light where the two ends are contrasting while there exists a continuum of colors in between, made of intermediate phenotypes. The loops denote the continuous withdrawal and merging of diversified hybrid phenotypes into the central band.

## 4 Conclusion and prospects

The novelty of this work lies in its integrated qualitative to quantitative evaluation of representative cell population in EMT to address their hidden dynamism embedded in the cellular plasticity. In this context present work demonstrated that highly variable phenotypic plasticity in a population is not independent but follows a trend defined by laws of probability. It also translated the known molecular facts of EMT on the cellular level endorsing their implication on morphological transitions. However, as this study has been performed on representative cell populations, the knowledge of the transition occurring at the tissue level is still quite limited. But, this study has definitely created a futuristic interface for value addition to histopathological and molecular pathology practices in addressing ambiguities related to assessment of EMT and associated cellular plasticity in the main stream diagnostic practices. Lastly, our model shows at later stages of EMT progression, the predominance of the mesenchymal/forming phenotypes. Even at these stages, some contributory cells (epithelial) continue to reappear from forming phenotypes ( $\delta \rightarrow \alpha$  in 24 - 48 h and  $\varepsilon \rightarrow \alpha$  in 48 - 72 h). Thus the cells advancing into EMT (even with the given experimental limitation) demonstrate the reappearance of epithelial phenotypes which may be an implicit indication of low but simultaneous occurrence of MET.

## Author disclosure statement

No competing financial interests exist.

## Acknowledgements

Funding for this research was provided by Ministry of Human Resource Development, Government of India (Sanction

letter no. F. NO. 4-23/2014 - TS.I, dated: 14.02.2014) through Indian Institute of Technology, Kharagpur and Department of Biotechnology, Government of India (Sanction letter no. BT/PR7961/MED/32/280/2013, dated: 18.06.2014).

We acknowledge Dr. Maneesha Inamdar, Jawaharlal Nehru Center for Advanced Scientific Research, Bangalore, India for helping us to fine-tune the EMT induction protocol. We would like to extend our sincere regards to Dr. Milind Vaidya, Advanced Centre for Treatment, Research and Education in Cancer, Mumbai, India for providing us AW13516 cell line. We also thank Sri Phani Krishna Karri and Monika Rajput, SMST, IIT Kharagpur for their valuable suggestions during the work.

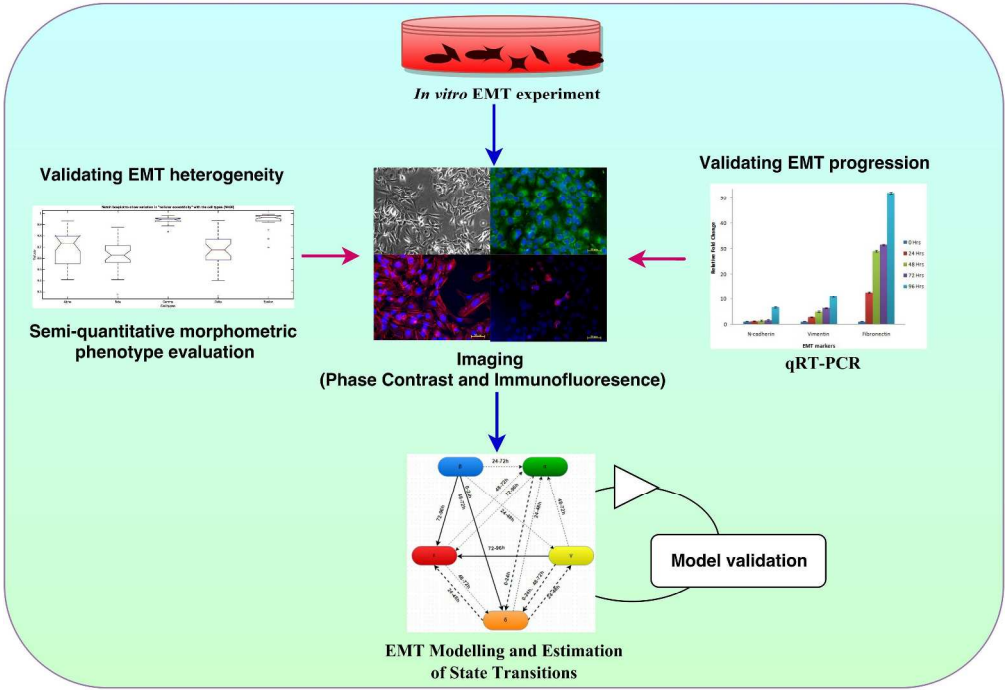
## References

- 1 T. D. Price, A. Qvarnström and D. E. Irwin, *Proceedings of the Royal Society of London B: Biological Sciences*, 2003, **270**, 1433–1440.
- 2 S. Tyler, *Integrative and comparative biology*, 2003, **43**, 55–63.
- 3 R. Kalluri and R. A. Weinberg, *The Journal of clinical investigation*, 2009, **119**, 1420.
- 4 E. D. Hay, *Epithelial-mesenchymal interactions*, 1968, **2**, 31–35.
- 5 G. Greenburg and E. D. Hay, *The Journal of cell biology*, 1982, **95**, 333–339.
- 6 V. Arnoux, M. Nassour, A. L'Helgoualc'h, R. A. Hipskind and P. Savagner, *Molecular biology of the cell*, 2008, **19**, 4738–4749.
- 7 C. Yan, W. A. Grimm, W. L. Garner, L. Qin, T. Travis, N. Tan and Y.-P. Han, *The American journal of pathology*, 2010, **176**, 2247–2258.
- 8 R. Kalluri and E. G. Neilson, *Journal of Clinical Investigation*, 2003, **112**, 1776.
- 9 T. A. Wynn and T. R. Ramalingam, *Nature medicine*, 2012, **18**, 1028–1040.
- 10 B. M. Grabias and K. Konstantopoulos, *The FASEB Journal*, 2012, **26**, 4131–4141.
- 11 E. L. Heinrich, T. C. Walser, K. Krysan, E. L. Licican, J. L. Grant, N. L. Rodriguez and S. M. Dubinett, *Cancer Microenvironment*, 2012, **5**, 5–18.
- 12 A.-P. Morel, M. Lièvre, C. Thomas, G. Hinkal, S. Ansieau and A. Puisieux, *PloS one*, 2008, **3**, e2888.
- 13 S. A. Mani, W. Guo, M.-J. Liao, E. N. Eaton, A. Ayyanan, A. Y. Zhou, M. Brooks, F. Reinhard, C. C. Zhang, M. Shipitsin *et al.*, *Cell*, 2008, **133**, 704–715.
- 14 K. Polyak and R. A. Weinberg, *Nature Reviews Cancer*, 2009, **9**, 265–273.
- 15 C. Scheel and R. A. Weinberg, *Seminars in cancer biology*, 2012, pp. 396–403.
- 16 J. Yang, S. A. Mani, J. L. Donaher, S. Ramaswamy, R. A. Itzyk-

- son, C. Come, P. Savagner, I. Gitelman, A. Richardson and R. A. Weinberg, *Cell*, 2004, **117**, 927–939.
- 17 J. P. Thiery, H. Acloque, R. Y. Huang and M. A. Nieto, *cell*, 2009, **139**, 871–890.
  - 18 J. H. Tsai and J. Yang, *Genes & development*, 2013, **27**, 2192–2206.
  - 19 D. Yao, C. Dai and S. Peng, *Molecular Cancer Research*, 2011, **9**, 1608–1620.
  - 20 A. Voulgari and A. Pintzas, *Biochimica et Biophysica Acta (BBA)-Reviews on Cancer*, 2009, **1796**, 75–90.
  - 21 M. K. Jolly, M. Boareto, B. Huang, D. Jia, M. Lu, J. N. Onuchic, H. Levine and E. Ben-Jacob, *arXiv preprint arXiv:1505.07494*, 2015.
  - 22 N. Bednarz-Knoll, C. Alix-Panabières and K. Pantel, *Cancer and Metastasis Reviews*, 2012, **31**, 673–687.
  - 23 J. Cursons, K.-J. Leuchowius, M. Waltham, E. Tomaskovic-Crook, M. Foroutan, C. P. Bracken, A. Redfern, E. J. Crampin, I. Street, M. J. Davis *et al.*, *Cell Communication and Signaling*, 2015, **13**, 26.
  - 24 G. Eades, Y. Yao, M. Yang, Y. Zhang, S. Chumsri and Q. Zhou, *Journal of Biological Chemistry*, 2011, **286**, 25992–26002.
  - 25 F. Z. Li, A. S. Dhillon, R. L. Anderson, G. McArthur and P. T. Ferraro, *Frontiers in oncology*, 2015, **5**, year.
  - 26 M. J. Schliekelman, A. Taguchi, J. Zhu, X. Dai, J. Rodriguez, M. Celikbas, Q. Zhang, A. Chin, C.-H. Wong, H. Wang *et al.*, *Cancer research*, 2015, **75**, 1789–1800.
  - 27 R. Y. Huang, M. Wong, T. Tan, K. Kuay, A. Ng, V. Chung, Y. Chu, N. Matsumura, H. Lai, Y. Lee *et al.*, *Cell death & disease*, 2013, **4**, e915.
  - 28 B. J. Van Denderen and E. W. Thompson, *Nature*, 2013, **493**, 487–488.
  - 29 P. Savagner, *Current topics in developmental biology*, 2015, **112**, 273–300.
  - 30 D. Tarin, *Cancer research*, 2005, **65**, 5996–6001.
  - 31 J. J. Christiansen and A. K. Rajasekaran, *Cancer research*, 2006, **66**, 8319–8326.
  - 32 M. H. Chui, *International Journal of Cancer*, 2013, **132**, 1487–1495.
  - 33 M. Iwatsuki, K. Mimori, T. Yokobori, H. Ishi, T. Beppu, S. Nakamori, H. Baba and M. Mori, *Cancer science*, 2010, **101**, 293–299.
  - 34 F. J. Carmona, V. Davalos, E. Vidal, A. Gomez, H. Heyn, Y. Hashimoto, M. Vizoso, A. Martinez-Cardus, S. Sayols, H. J. Ferreira *et al.*, *Cancer research*, 2014, **74**, 5608–5619.
  - 35 Z. Tan, W. Lu, X. Li, G. Yang, J. Guo, H. Yu, Z. Li and F. Guan, *Journal of proteome research*, 2014, **13**, 2783–2795.
  - 36 P.-J. P. Aspuria, S. Y. Lunt, L. Våremo, L. Vergnes, M. Gozo, J. A. Beach, B. Salumbides, K. Reue, W. R. Wiedemeyer, J. Nielsen *et al.*, *Cancer & metabolism*, 2014, **2**, 21.
  - 37 J. Li, L. Dong, D. Wei, X. Wang, S. Zhang and H. Li, *International journal of biological sciences*, 2014, **10**, 171.
  - 38 D. M. Gonzalez and D. Medici, *Science signaling*, 2014, **7**, re8.
  - 39 S. Lamouille, J. Xu and R. Derynck, *Nature reviews Molecular cell biology*, 2014, **15**, 178–196.
  - 40 Y. Teng, M. Zeisberg and R. Kalluri, *Journal of Clinical Investigation*, 2007, **117**, 304.
  - 41 C. Scanlon, E. Van Tubergen, R. Inglehart and N. D'Ávila, *Journal of dental research*, 2012, 0022034512467352.
  - 42 X.-J. Tian, H. Zhang and J. Xing, *Biophysical journal*, 2013, **105**, 1079–1089.
  - 43 J. Zhang, X.-J. Tian, H. Zhang, Y. Teng, R. Li, F. Bai, S. Elankumaran and J. Xing, *Science signaling*, 2014, **7**, ra91–ra91.
  - 44 D. Jia, M. K. Jolly, M. Boareto, P. Parsana, S. M. Mooney, K. J. Pienta, H. Levine and E. Ben-Jacob, *Oncotarget*, 2015, **5**, year.
  - 45 M. K. Jolly, B. Huang, M. Lu, S. A. Mani, H. Levine and E. Ben-Jacob, *Journal of The Royal Society Interface*, 2014, **11**, 20140962.
  - 46 S. K. Wu, G. A. Gomez, M. Michael, S. Verma, H. L. Cox, J. G. Lefevre, R. G. Parton, N. A. Hamilton, Z. Neufeld, A. S. Yap *et al.*, *Nature cell biology*, 2014, **16**, 167–178.
  - 47 J. Haynes, J. Srivastava, N. Madson, T. Wittmann and D. L. Barber, *Molecular biology of the cell*, 2011, **22**, 4750–4764.
  - 48 J. Ivaska, H.-M. Pallari, J. Nevo and J. E. Eriksson, *Experimental cell research*, 2007, **313**, 2050–2062.
  - 49 M. G. Mendez, S.-I. Kojima and R. D. Goldman, *The FASEB Journal*, 2010, **24**, 1838–1851.
  - 50 R. Pankov and K. M. Yamada, *Journal of cell science*, 2002, **115**, 3861–3863.
  - 51 J. M. Halbleib and W. J. Nelson, *Genes & development*, 2006, **20**, 3199–3214.
  - 52 L. R. Rabiner, *Proceedings of the IEEE*, 1989, **77**, 257–286.
  - 53 K. J. Livak and T. D. Schmittgen, *methods*, 2001, **25**, 402–408.
  - 54 N. Nasreen, K. A. Mohammed, K. K. Mubarak, M. A. Baz, O. A. Akindipe, S. Fernandez-Bussy and V. B. Antony, *American Journal of Physiology-Lung Cellular and Molecular Physiology*, 2009, **297**, L115–L124.
  - 55 S. Das, B. N. Becker, F. M. Hoffmann and J. E. Mertz, *BMC cell biology*, 2009, **10**, 94.
  - 56 Z.-D. Lv, B. Kong, J.-G. Li, H.-L. Qu, X.-G. Wang, W.-H. Cao, X.-Y. Liu, Y. Wang, Z.-C. Yang, H.-M. Xu *et al.*, *Oncology reports*, 2013, **29**, 219–225.
  - 57 M. Maeda, K. R. Johnson and M. J. Wheelock, *Journal of cell science*, 2005, **118**, 873–887.
  - 58 C. D. Nobes and A. Hall, *Cell*, 1995, **81**, 53–62.
  - 59 B. Short, *The Journal of cell biology*, 2012, **196**, 301–301.
  - 60 M. L. Ackland, D. F. Newgreen, M. Fridman, M. C. Waltham, A. Arvanitis, J. Minichiello, J. T. Price and E. W. Thompson,

- Laboratory investigation, 2003, **83**, 435–448.
- 61 B. Willipinski-Stapelfeldt, S. Riethdorf, V. Assmann, J. Heukeshoven and K. Pantel, *Clinical Cancer Research*, 2005, **11**, 8006–8014.
  - 62 E. Korsching, J. Packeisen, C. Liedtke, D. Hungermann, P. Wülfing, P. J. van Diest, B. Brandt, W. Boecker and H. Buerger, *The Journal of pathology*, 2005, **206**, 451–457.
  - 63 M. I. Kokkinos, R. Wafai, M. K. Wong, D. F. Newgreen, E. W. Thompson and M. Waltham, *Cells Tissues Organs*, 2007, **185**, 191–203.
  - 64 B. Eckes, E. Colucci-Guyon, H. Smola, S. Nodder, C. Babinet, T. Krieg and P. Martin, *Journal of cell science*, 2000, **113**, 2455–2462.
  - 65 J. Wei, G. Xu, M. Wu, Y. Zhang, Q. Li, P. Liu, T. Zhu, A. Song, L. Zhao, Z. Han *et al.*, *Anticancer research*, 2008, **28**, 327–334.
  - 66 V. Tirino, R. Camerlingo, K. Bifulco, E. Irollo, R. Montella, F. Paino, G. Sessa, M. Carrierio, N. Normanno, G. Rocco *et al.*, *Cell death & disease*, 2013, **4**, e620.
  - 67 N. E. Wikner, K. A. Persichitte, J. B. Baskin, L. D. Nielsen and R. A. Clark, *Journal of investigative dermatology*, 1988, **91**, 207–212.
  - 68 J. Park and J. E. Schwarzbauer, *Oncogene*, 2014, **33**, 1649–1657.
  - 69 M. J. Wheelock, Y. Shintani, M. Maeda, Y. Fukumoto and K. R. Johnson, *Journal of cell science*, 2008, **121**, 727–735.
  - 70 P. Suresh and L. Nathawat, *International Journal of Pharmacy and Pharmaceutical Sciences*, 2014, **6**, 97–102.
  - 71 R. B. Hazan, G. R. Phillips, R. F. Qiao, L. Norton and S. A. Aaronson, *The Journal of cell biology*, 2000, **148**, 779–790.
  - 72 W. Shih and S. Yamada, *Cell adhesion & migration*, 2012, **3**, 513–517.
  - 73 L. D. Derycke and M. E. Bracke, *International Journal of Developmental Biology*, 2004, **48**, 463–476.
  - 74 H. Kasai, J. T. Allen, R. M. Mason, T. Kamimura and Z. Zhang, *Respiratory research*, 2005, **6**, 56.
  - 75 F. Zhang, M. Mönkkönen, S. Roth and M. Laiho, *Experimental cell research*, 2002, **281**, 190–196.
  - 76 S. B. Jakowlew, *Cancer and Metastasis Reviews*, 2006, **25**, 435–457.
  - 77 J.-J. Lebrun, *ISRN molecular biology*, 2012, **2012**, year.
  - 78 J. M. Zarzynska, *Mediators of inflammation*, 2014, **2014**, year.
  - 79 S. Ehata, A. Hanyu, M. Hayashi, H. Aburatani, Y. Kato, M. Fujime, M. Saitoh, K. Miyazawa, T. Imamura and K. Miyazono, *Cancer research*, 2007, **67**, 9694–9703.
  - 80 R. French and R. Clarkson, *J Stem Cell Res Ther S*, 2012, **7**, year.
  - 81 M. Atena, A. M. Reza and G. Mehran, *Stem Cell Discovery*, 2014, **4**, 83.
  - 82 C. J. Eaves, *Nature*, 2008, **456**, 581–582.
  - 83 W. L. Tam and R. A. Weinberg, *Nature medicine*, 2013, **19**, 1438–1449.
  - 84 M. El-Soda, M. Malosetti, B. J. Zwaan, M. Koornneef and M. G. Aarts, *Trends in plant science*, 2014, **19**, 390–398.





1412x975mm (72 x 72 DPI)